ELSEVIER

Engineering Geology 58 (2000) 271–289

ENGINEERING GEOLOGY

www.elsevier.nl/locate/enggeo

A method for producing digital probabilistic seismic landslide hazard maps

Randall W. Jibson *, Edwin L. Harp, John A. Michael

US Geological Survey, Box 25046, MS 966, Denver Federal Center, Denver, CO 80225, USA

Received 5 January 1999; accepted for publication 7 March 2000

Abstract

The 1994 Northridge, California, earthquake is the first earthquake for which we have all of the data sets needed to conduct a rigorous regional analysis of seismic slope instability. These data sets include: (1) a comprehensive inventory of triggered landslides, (2) about 200 strong-motion records of the mainshock, (3) 1:24 000-scale geologic mapping of the region, (4) extensive data on engineering properties of geologic units, and (5) high-resolution digital elevation models of the topography. All of these data sets have been digitized and rasterized at 10 m grid spacing using ARC/INFO GIS software on a UNIX computer. Combining these data sets in a dynamic model based on Newmark's permanent-deformation (sliding-block) analysis yields estimates of coseismic landslide displacement in each grid cell from the Northridge earthquake. The modeled displacements are then compared with the digital inventory of landslides triggered by the Northridge earthquake to construct a probability curve relating predicted displacement to probability of failure. This probability function can be applied to predict and map the spatial variability in failure probability in any ground-shaking conditions of interest. We anticipate that this mapping procedure will be used to construct seismic landslide hazard maps that will assist in emergency preparedness planning and in making rational decisions regarding development and construction in areas susceptible to seismic slope failure.

Keywords: Earthquakes; GIS; Hazard mapping; Landslides; Seismic hazards

1. Introduction

Landslides are one of the most damaging collateral hazards associated with earthquakes. In fact, damage from triggered landslides has sometimes exceeded damage directly related to strong shaking and fault rupture. Seismically triggered landslides damage and destroy homes and other structures, block roads, sever pipelines and other utility lifelines, and block stream drainages. Estimating where and in what shaking conditions earthquakes are likely to trigger landslides is a key element in regional seismic hazard assessment. Until now, however, we have lacked the data necessary to make such forecasts in a rigorous way.

Factors contributing to slope failure at a specific site are generally complex and difficult to assess with confidence; therefore, regional analysis of a large group of landslides triggered in a well-documented earthquake is useful to estimate general conditions related to failure. The 1994 Northridge, California, earthquake (magnitude-6.7) presents the ideal case for such an analysis because all of the data sets required for detailed regional analysis

* Corresponding author. Tel.: +1-303-273-8577;
fax: +1-303-273-8600.
E-mail address: jibson@usgs.gov (R.W. Jibson)

0013-7952/00/$ - see front matter © 2000 Elsevier Science B.V. All rights reserved.
PII: S0013-7952(00)00039-9

of slope failures are available. We present here a method to map the spatial distribution of probabilities of seismic slope failure in any set of ground-shaking conditions of interest. The method was first developed and calibrated using data from the 1994 Northridge earthquake in the Oat Mountain 7 1/2′ quadrangle, on the northern edge of San Fernando Valley near Los Angeles, California (Jibson et al., 1998). A limitation of that initial calibration was that the effects of strong-motion attenuation could not be rigorously accounted for by modeling a single quadrangle that was effectively saturated with high-amplitude ground motion. Therefore, in this paper, we recapitulate the original methodology and recalibrate it using a much larger data set covering six 7 1/2′ quadrangles, an area large enough to encompass significant variations in ground shaking.

2. Modeling method

We model the dynamic performance of slopes using the permanent-displacement analysis developed by Newmark (1965). Wilson and Keefer (1983) showed that using Newmark's method to model the dynamic behavior of landslides on natural slopes yields reasonable and useful results. Wieczorek et al. (1985) subsequently produced an experimental map showing seismic landslide susceptibility in San Mateo County, California, using classification criteria based on Newmark's method. Wilson and Keefer (1985) also used Newmark's method as a basis for a broad regional assessment of seismic slope stability in the Los Angeles, California, area.

Newmark's method models a landslide as a rigid friction block that slides on an inclined plane (Fig. 1). The block has a known critical (or yield) acceleration, a_c, which is simply the threshold base acceleration required to overcome shear resistance and initiate sliding. The analysis calculates the cumulative permanent displacement of the block relative to its base as it is subjected to the effects of an earthquake acceleration–time history.

In the analysis, an acceleration–time history of interest is selected, and the critical acceleration of the slope to be modeled is superimposed [Fig. 2(A)]. Accelerations below this level cause

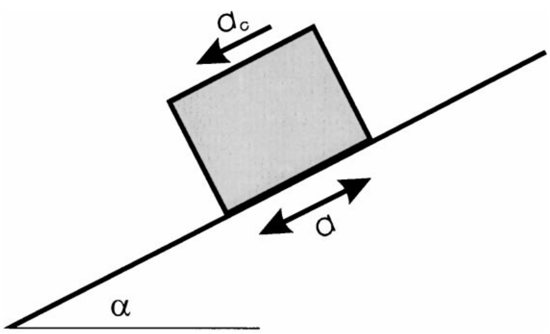

Fig. 1. Sliding-block model used for Newmark analysis. The potential landslide is modeled as a block resting on a plane inclined at an angle (α) from the horizontal. The block has a known critical (yield) acceleration (a_c), the base acceleration required to overcome shear resistance and initiate sliding with respect to the base. The block is subjected to a base acceleration (a) representing the earthquake shaking.

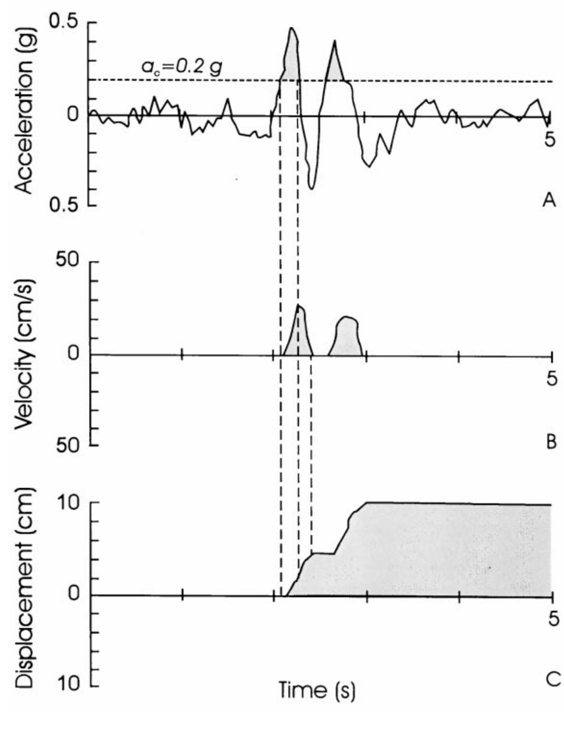

Fig. 2. Demonstration of the Newmark-analysis algorithm (adapted from Wilson and Keefer, 1983). (A) Earthquake acceleration–time history with critical acceleration (horizontal dashed line) of 0.20g superimposed. (B) Velocity of landslide block versus time. (C) Displacement of landslide block versus time.

no permanent displacement of the block. Those portions of the record that exceed the critical acceleration are integrated once to obtain the velocity profile of the block [Fig. 2(B)]; a second integration is performed to obtain the cumulative displacement history of the block [Fig. 2(C)]. The user then judges the significance of the displacement. Newmark's method is based on a fairly simple model of rigid-body displacement, and thus it does not necessarily precisely predict measured landslide displacements in the field. Rather, Newmark displacement is a useful index of how a slope is likely to perform during seismic shaking.

Newmark (1965) showed that the critical acceleration of a potential landslide block is a simple function of the static factor of safety and the landslide geometry, expressed as

$$a_c = (\mathrm{FS}-1)g \sin \alpha, \quad (1)$$

where a_c is the critical acceleration in terms of g, the acceleration of Earth's gravity; FS is the static factor of safety; and α is the angle from the horizontal that the center of mass of the potential landslide block first moves, which can generally be approximated as the slope angle. Thus, conducting a Newmark analysis requires knowing the static factor of safety and the slope angle and selecting an earthquake strong-motion record.

3. Location

We first developed the methodology (Jibson et al., 1998) in the Oat Mountain 7 1/2′ quadrangle, which includes parts of the northern San Fernando Valley and Santa Susana Mountains. For this broader recalibration, we use data from six quadrangles in the same area: the Oat Mountain, Santa Susana, Simi, Piru, Val Verde, and Newhall 7 1/2′ quadrangles (Fig. 3). These quadrangles lie immediately north and west of the Northridge earthquake epicenter and contain dense concentrations of triggered landslides (Harp and Jibson, 1995, 1996). The topography ranges from flat areas in the San Fernando, Simi, and Santa Clara River Valleys to nearly vertical slopes in the Santa Susana Mountains and the mountains north of the Santa Clara River (Fig. 3). Predominant geologic units in the area include uncemented to weakly cemented late Tertiary clastic sediments as well as well-cemented Cretaceous sandstone.

The large majority of landslides triggered in 1994 were shallow (1–2 m deep), disrupted falls and slides in rock and debris. The weakly cemented Tertiary sedimentary rocks in the area produced most of these slides, which occurred in particularly dense concentrations in steeply incised canyons eroded into the relatively young sediments that have been uplifted and deformed rapidly in the recent geologic past.

Very few of the triggered landslides involved reactivation of pre-existing landslide masses. However, many of the shallow, disrupted slides initiated on steep slopes that undoubtedly have produced landslides in the past. A detailed study of the Santa Susana quadrangle showed that mapped Quaternary landslides occupied 7.1% of the quadrangle, but only 3.3% of the landslides triggered by the Northridge earthquake occurred in the mapped Quaternary landslides (Parise and Jibson, 1997, this volume). Thus, far from having an increased susceptibility to landsliding, mapped Quaternary landslides produced new landslides at less than half the average rate of all the units in the quadrangle. This is probably because landslides shown on geologic maps are large, deep, coherent masses that did not experience significant internal disruption during past movement.

In 1971, the magnitude-6.5 San Fernando earthquake occurred about 25 km northeast of the 1994 Northridge epicenter. Similar in size to the Northridge earthquake, the 1971 earthquake also triggered numerous shallow landslides that were concentrated in the same geologic units that produced most of the 1994 landslides (Morton, 1975). Most of the 1971 landslides were in the San Gabriel Mountains, east of the current study area, but several landslides were triggered in the eastern part of the Oat Mountain quadrangle, which formed the western limit of the 1971 landslides (Morton, 1975).

4. Overview of the mapping methodology

The Northridge earthquake is the first earthquake for which we have all of the data sets needed to conduct a detailed regional analysis of factors related to triggered landsliding. These data sets

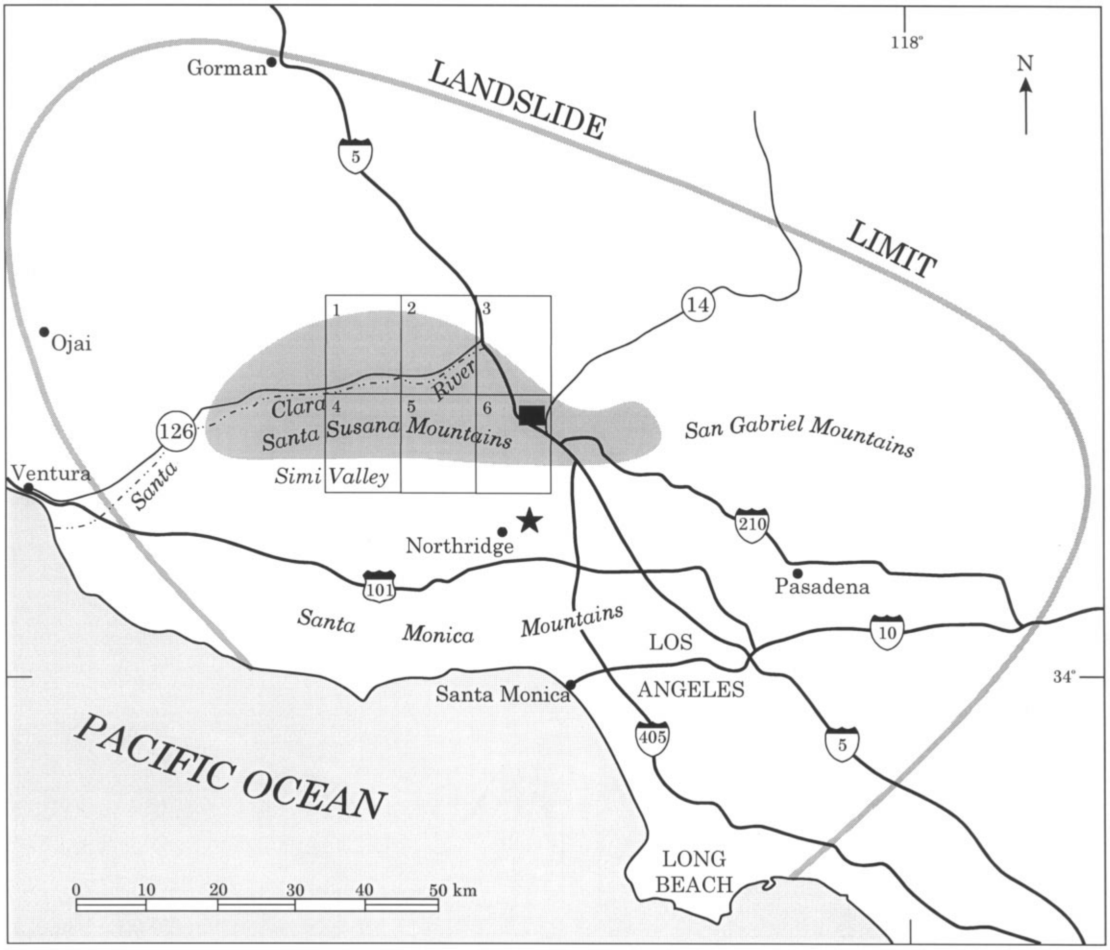

Fig. 3. Location of the Piru (1), Val Verde (2), Newhall (3), Simi (4), Santa Susana (5), and Oat Mountain (6) 7 1/2′quadrangles, California. The bold gray line indicates the limit of landslides triggered by Northridge earthquake; the shaded area shows the zone of greatest landslide concentration; the star shows the Northridge epicenter; the black box shows the sample area referred to in subsequent figures.

include (1) a comprehensive inventory of triggered landslides (Harp and Jibson, 1995, 1996), (2) about 200 strong-motion records of the main shock recorded throughout the region of landsliding, (3) detailed (1:24 000-scale) geologic mapping of the region, (4) extensive data on engineering properties of geologic units, and (5) high-resolution digital elevation models of the topography. All of these data sets have been digitized and rasterized at 10 m grid spacing using ARC/INFO geographic information system (GIS) software. Combining these data sets in a dynamic model based on Newmark's permanent-deformation (sliding-block) analysis yields estimates of coseismic landslide displacement in each grid cell from the Northridge earthquake. The modeled displacements are then compared with the digital inventory of landslides triggered by the Northridge earthquake to construct a probability curve relating predicted displacement to probability of failure. Once calibrated with Northridge data, the probability function can be applied to predict the spatial variability of failure probability in any ground-shaking scenario of interest. Because the resulting hazard maps are digital, they can be updated and revised with additional data that become available, and custom maps that model any ground-shaking conditions of interest can be produced when needed.

Fig. 4 is a flowchart showing the sequential steps involved in the hazard-mapping procedure. Data layers consist of 10 m grids of each of the quadrangles. The sequence is relatively straightforward:

1. Compute the static factor of safety (ratio of resisting to driving forces).
   (A) Using compiled shear-strength data, assign representative shear strengths to each unit on the geologic map, which yields friction (ϕ') and cohesion (c') grids.
   (B) Produce a slope map from the digital elevation model (DEM).
   (C) Combine shear-strength and slope data in a factor-of-safety equation to estimate static factors of safety in each grid cell.
2. Compute the critical acceleration by combining the factor-of-safety grid with the slope grid to yield the critical acceleration grid, which represents seismic landslide susceptibility.
3. Estimate Newmark displacements from the Northridge earthquake using an empirical regression equation to combine the critical-acceleration grid with the grid containing shaking-intensity values from the Northridge earthquake.
4. Construct a curve to estimate probability of slope failure as a function of Newmark displacement.
   (A) Compare the map of landslides triggered by the Northridge earthquake to the Newmark-displacement grid.
   (B) For sequential intervals of Newmark displacement, compute the proportion of cells containing landslides.
   (C) Plot the proportion of failed slopes in each interval as a function of Newmark displacement, and fit a regression curve.
5. Generate maps showing probability of seismic slope failure in any shaking scenario of interest.
   (A) Estimate Newmark displacements by combining a ground-shaking grid of interest with the critical acceleration grid, as in step 3.
   (B) Estimate probabilities of failure using the calibrated regression curve from step 4.

5. Details of the mapping methodology

In the sections that follow, each of the steps outlined above is discussed in detail.

5.1. Computing the static factor of safety

The dynamic stability of a slope, in the context of Newmark's method, is related to its static

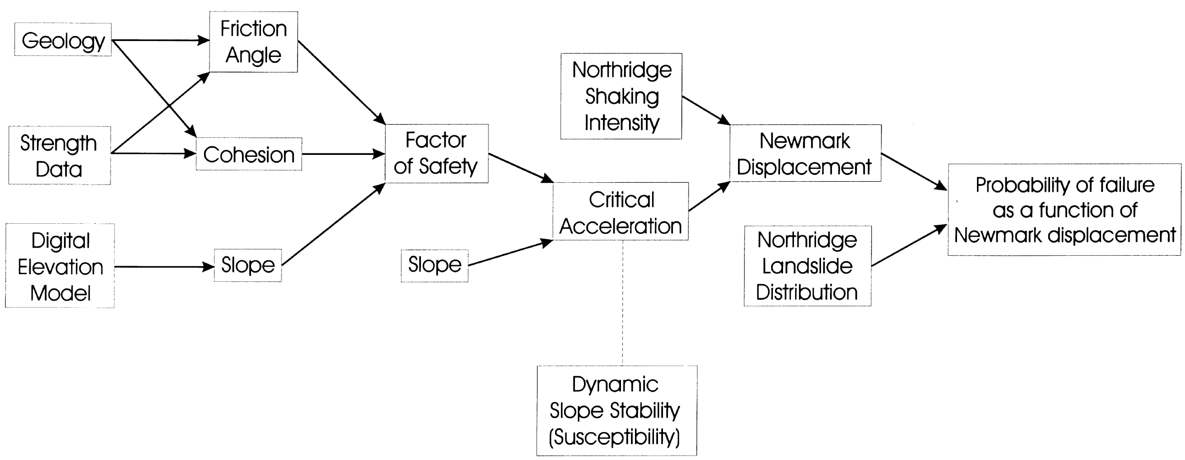

Fig. 4. Flow chart showing steps involved in producing a seismic landslide hazard map.

stability [see Eq. (1)]; therefore, the static factor of safety for each grid cell must be estimated. For purposes of regional analysis, we use a relatively simple limit-equilibrium model of an infinite slope in material having both frictional and cohesive strength. The static factor of safety (*FS*) in these conditions is

$$\mathrm{FS}=\frac{c'}{\gamma t \sin \alpha}+\frac{\tan \phi'}{\tan \alpha}-\frac{m\gamma_{\mathrm{w}} \tan \phi'}{\gamma \tan \alpha}, \qquad (2)$$

where ϕ' is the effective friction angle, c' is the effective cohesion, α is the slope angle, γ is the material unit weight, γ_{w} is the unit weight of water, t is the slope-normal thickness of the failure slab, and m is the proportion of the slab thickness that is saturated. The equation is written so that the first term on the right-hand side accounts for the cohesive component of the strength, the second term accounts for the frictional component, and the third term accounts for the reduction in frictional strength due to pore pressure. The southern California area has a semi-arid climate, and virtually no rain had fallen in the region for several months; thus, the fractured, primarily coarse-grained surficial slope materials were very dry. Therefore, no pore-water pressure is included ($m=0$) in this calibration, and the third term drops from the equation. For simplicity, the product γt is taken to be 38.3 kPa (800 lbs/ft^2), which reflects a typical unit weight of 15.7 kN/m^3 (100 lbs/ft^3) and slab thickness of 2.4 m (8 ft), representative of typical Northridge failures. The relatively low unit weight applies to the near-surface material in the weathered zone that is fractured, dilated, and has soil-like properties. The factor of safety, then, is calculated by inserting values from the friction, cohesion, and slope-angle grids into Eq. (2).

5.1.1. Geologic map

Digital geologic maps of the six quadrangles form the basis for assigning material properties throughout the area (Fig. 5). We used the 1:24 000-scale digital geologic maps of Yerkes and Campbell (1993, 1995a–h, 1997a–c). Representative values of the frictional and cohesive

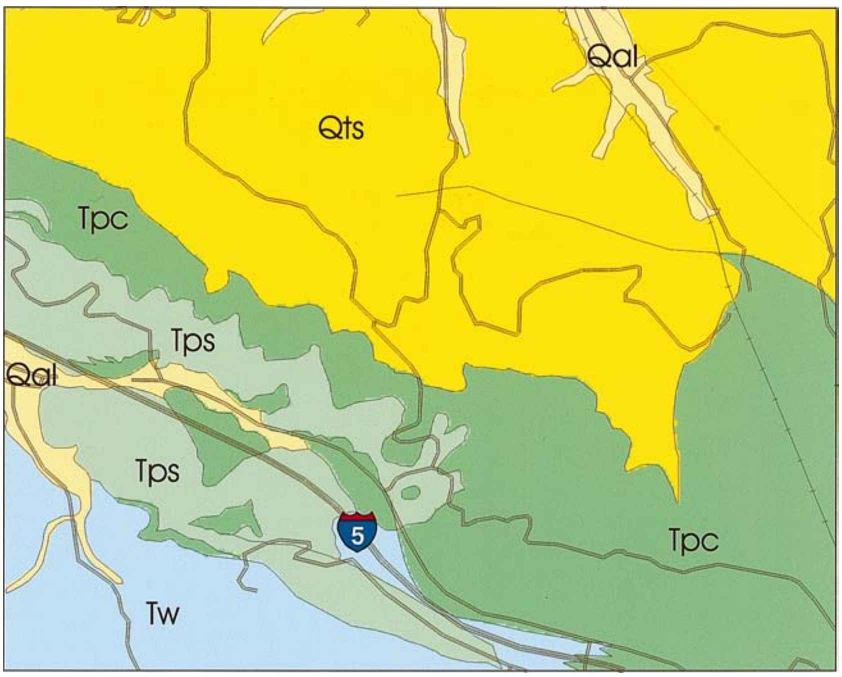

Fig. 5. Geologic map of part of the Oat Mountain quadrangle (location shown in Fig. 3).

components of shear strength were assigned to each geologic unit.

5.1.2. Shear-strength data

Representative shear-strength values for geologic units were selected based on (1) compilation of numerous direct-shear test results from local consultants, (2) the judgment of several experienced geotechnical engineers and geologists in the region, and (3) the constraint that the computer slope model be statically stable. Assigning shear strengths admittedly is a somewhat subjective process, but using several different sources of data and approaches provides a reasonably consistent result.

We compiled results from hundreds of direct-shear tests on samples from a variety of geologic units in the six quadrangles and the surrounding region. In addition, we queried several experienced professionals from the local practicing and regulatory communities regarding representative shear-strength values for seismic conditions. There was a broad agreement among these sources of information regarding the relative strengths of the various geologic units, which allowed us to rank the units by strength and to approximate strength differences between units (i.e. unit A is about 10% stronger, on average, than unit B). In the initial iteration of the model, we assigned strengths near the middle of the ranges represented in our sources of information, and we adjusted strengths where needed to preserve the documented differences in strengths between units.

The six quadrangles analyzed have areas of very steep terrain, and the first factor-of-safety iteration yielded factors of safety less than 1 (indicating static instability) in some grid cells in steep areas. Our last constraint on assigning shear strengths to units, then, was that the model be statically stable, which simply means that the slopes are not moving before the earthquake shaking occurs. We incrementally increased strengths of units having statically unstable cells, and then adjusted strengths of other units to preserve the observed strength differences between units. We did this iteratively until all slopes less than 60° were statically stable. A very small number (roughly a few dozen cells out of several million) of slopes steeper than 60° remained unstable, even at rather high strengths; therefore, we assigned a minimal factor of safety of 1.01, barely above equilibrium, to these slopes to avoid increasing the strengths beyond realistic levels.

Table 1 shows the strengths assigned to geologic units. These strengths clearly should be considered peak strengths and represent the higher end of the range of probable strength variation within a given unit because they are strengths required to maintain stability in the very steepest of slopes within that unit. As will become clear later in the analysis, the absolute value of the assigned strength is less important than the relative strength differences between units, and those differences are reasonably well constrained in a regional sense. Fig. 6 shows the friction [Fig. 6(A)] and cohesion [Fig. 6(B)] values assigned to the geologic units in a part of the area.

Peak strengths were also assigned to Quaternary landslides mapped on the geologic map. These landslides are primarily large, deep slide masses in bedrock that remained fairly coherent and did not significantly disrupt the surficial material where most of the triggered landslides occurred.

5.1.3. Digital elevation model

The 10 m digital elevation model (DEM) was produced by high-resolution scanning of the original USGS contour plates of the 1:24 000-scale quadrangle maps (Fig. 7). We selected a 10 m scanning resolution to preserve the subtle topographic features in which many landslides occur; too many topographic irregularities are lost in the more commonly used 30 m DEMs It must be remembered, however, that the DEM is simply a digital representation of the original contour map: higher-resolution scans produce DEMs that more faithfully reflect the published contour map, but they do not improve on any limitation that map may have.

5.1.4. Slope map

The slope map (Fig. 8) was produced by applying a simple algorithm to the DEM that compares the elevations of adjacent cells and computes the maximum slope. The slope map tends to underestimate some of the steepest slopes (steeper than

Table 1
Shear strengths assigned to geologic formations in the six quadrangles of the study area[a]

Unit name (description)	Oat Mountain	Santa Susana	Simi Valley	Newhall	Val Verde	Piru	ϕ' (°)	c' (lbs/ft^2)
Artificial fill	af		af	af	af	af	34	350
Artificial cut and fill	acf						34	350
Rockfall deposits	rf						34	350
Spoil from quarries	Qsp						34	350
Alluvium (young)	Qay						34	350
Pond deposits	Qp			Ql			34	350
Flood plain deposits						Qfp	34	350
Alluvium	Qal	Qal	Qal	Qal (1,2)	Qal	Qal	34	350
Older alluvium	Qao	Qao	Qao	Qao	Qao	Qao	34	350
Slope wash	Qsw	Qsw		Qsw			34	400
Caliche	Qc			Qc?			34	350
Landslide deposits	Qls	Qls	Qls	Qls	Qls	Qls	30	500
Terrace deposits	Qt	Qt	Qt	Qt	Qt	Qt	34	350
Fan and terrace deposits		Qft			Qf	Qf	34	350
Pacoima Fm. (ss/cg)				Qpa			34	400
Older terrace deposits	Qto			Qto			34	350
Old fanglomerate				Qfo			34	350
Saugus Fm.	QTs	Qs	Qs	Qs	Qs	Qs	34	400
Upper Member (silty breccia)	QTsu						34	450
Lower Member/Sunshine Ranch Fm.	QTsm	Qsm	Qsm				34	450
Saugus (Pelona Schist clasts)				Qsp	Qsp		34	400
Saugus (San Francisquito clasts)				Qss	Qss		34	400
Pico Fm.	Tp	QTp	QTp		Tp	Tp	32	500
Pico Fm. (?)	Tp?						34	500
Pico Fm. (ss/cg)	Tpc	QTpc		Tpc	Tpc	Tpc	34	500
Pico Fm. (silt)	Tps	QTps		Tps	Tps	Tps	30	500
Towsley Fm. (ss/shale)	Tw	Tw					34	550
Towsley Fm. (shale)	Tws	Tws		Tws	Tws	Tws	30	550
Towsley Fm. (ss)	Twc	Twc		Twc	Twc	Twc	34	550
Hasley Conglomerate					Twhc	Twhc	34	500
Castaic Fm. (ss)				Tcs	Tcs		34	400
Mint Canyon Fm. (ss)				Tmc			34	400
Mint Canyon Fm. (ss/clay)				Tmcl			32	400
Modelo Fm. (shale)	Tm	Tm	Tm			Tm	31	550
Modelo Fm. (shale/mud)	Tm1		Tm1			Tm1	31	550
Modelo Fm. (porc. shale)	Tm2	Tm2	Tm2			Tm2	31	550
Modelo Fm. (ss)	Tm3	Tm3	Tm3			Tm3	34	550
Modelo Fm. (shale)	Tm4	Tm4	Tm4			Tm4	31	550
Modelo Fm. (shale)						Tm5	31	550
Modelo Fm. (diatom. shale)	Tmd	Tmd					31	550
Modelo Fm. (shale)	Tms				Tms		31	550
Modelo Fm. (cg/ss)					Tmc		34	550
Topanga Fm. (ss)	Tt	Tt	Tt				34	550
Topanga Fm. (basalt)	Ttb	Ti					34	700
Topanga Fm. (shale)	Tt1						31	600
Topanga Fm. (ss)	Tt2						34	550
Topanga Fm. (shale)	Tt3						31	600
Topanga Fm. (ss)	Tt4						34	550
Conejo Volcanics (andesite/ basalt)			Tco				40	850
Conejo Volcanics (andesite)			Tcoa				40	900
Conejo Volcanics (basalt)			Tcob				40	800
Rincon Shale						Trn	30	400
Vaqueros Fm. (silt, ss)			Tv			Tv	33	600
Sespe Fm. (ss, cg)		Ts	Ts			Ts	33	550
Llajas Fm. (ss, silt, clay, cg)	Tl	Tl	Tl				33	600
Llajas Fm. (calc. ss, hard)	Tlc	Tlc					36	900
Santa Susana Fm. (clay shale)	Tss	Tss					30	700
Simi Conglomerate		Tsc					34	850
Simi Conglomerate (cg)	Tsc1						34	850
Simi Conglomerate (shale)	Tsc2						30	700
Simi Conglomerate (ss)	Tsc3						34	800
Chatsworth Fm. (ss)	Kc	Kc					40	1000

[a] ϕ': effective angle of internal friction; c': effective cohesion intercept; ss: sandstone; cg: conglomerate; 1 lb/ft^2 = 0.0479 kPa.

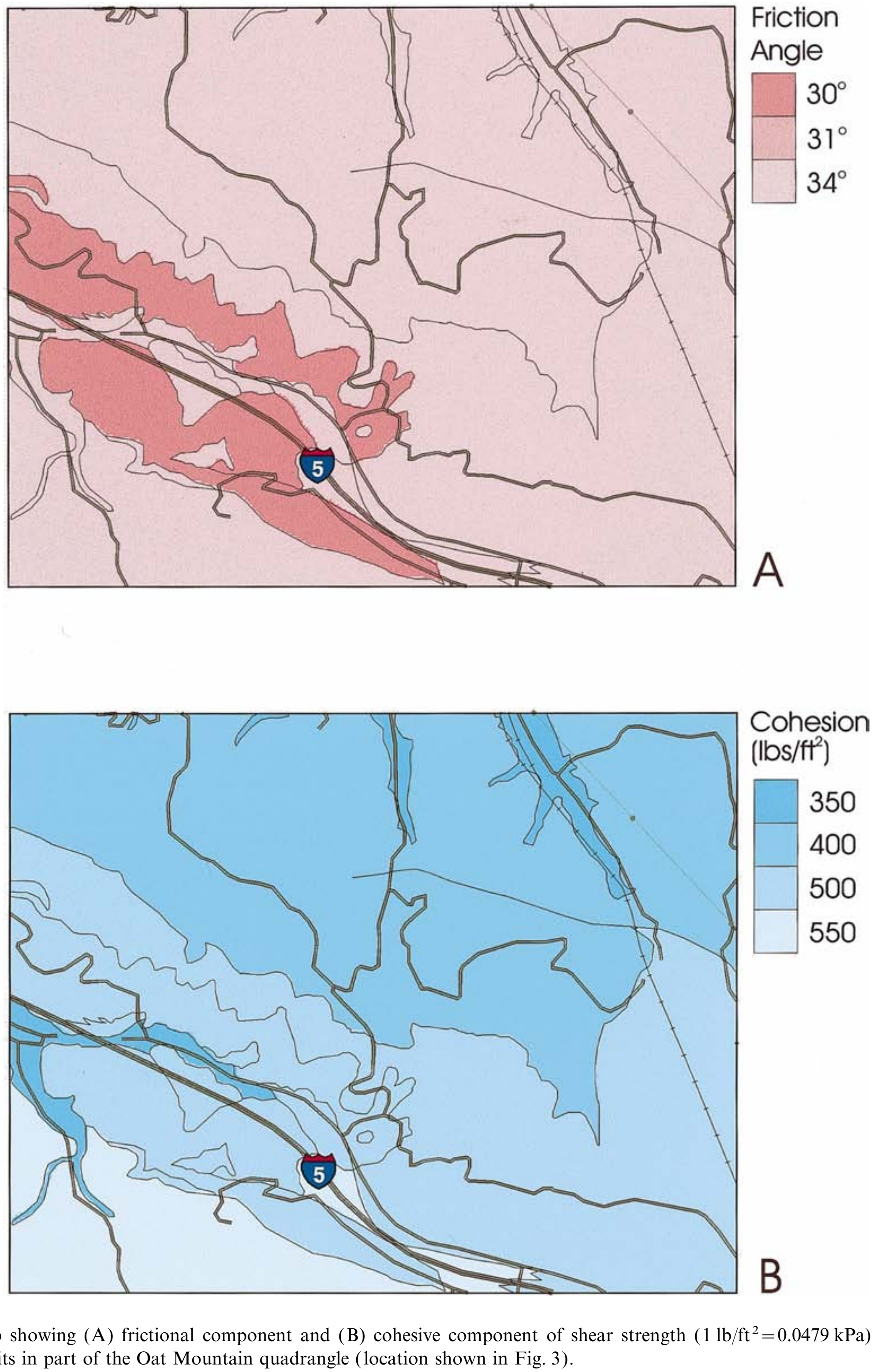

Fig. 6. Map showing (A) frictional component and (B) cohesive component of shear strength (1 lb/ft^2 = 0.0479 kPa) assigned to geologic units in part of the Oat Mountain quadrangle (location shown in Fig. 3).

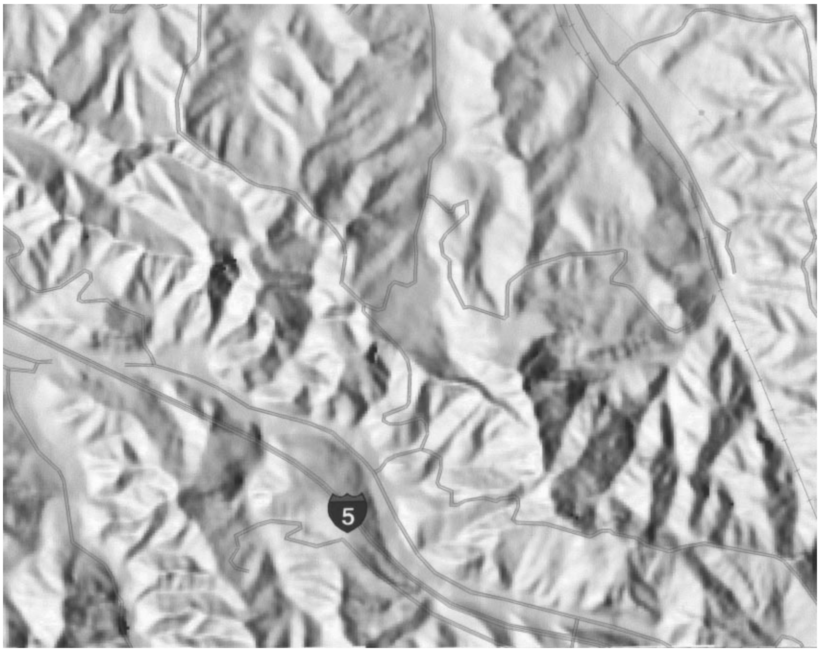

Fig. 7. Shaded-relief digital elevation model (DEM) of part of the Oat Mountain quadrangle (location shown in Fig. 3).

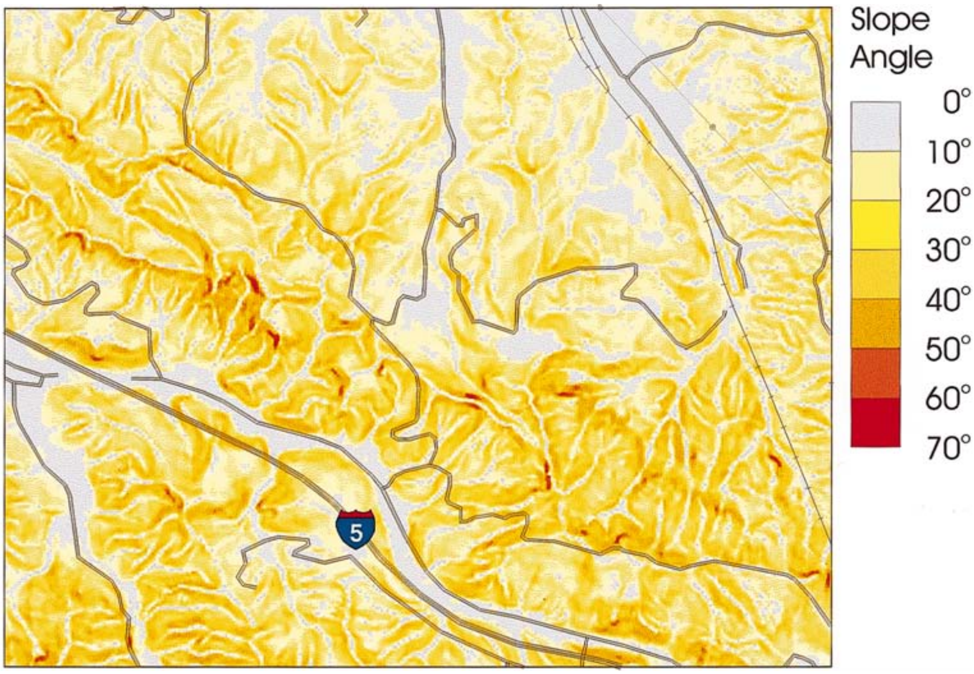

Fig. 8. Slope map derived from DEM of part of the Oat Mountain quadrangle (location shown in Fig. 3).

about 60°) primarily because such slopes are not well represented on the original contour map.

5.1.5. Factor-of-safety map

Fig. 9 shows a part of the factor-of-safety map resulting from combining these data layers (friction angle, cohesion, and slope) in Eq. (2). Factors of safety range from just greater than 1.0, for steep slopes in weak material, to more than 8 for flatter slopes in strong material.

5.2. Computing the critical acceleration

As indicated above, Newmark (1965) showed that the critical acceleration of a slope is a simple function of its static factor of safety and the slope angle [see Eq. (1)]. Therefore, producing a critical-acceleration grid is a simple matter of using Eq. (1) to combine the slope angle with the calculated factors of safety (Fig. 10).

Within the context of the Newmark-displacement analysis, critical (or yield) acceleration uniquely describes the dynamic stability of a slope. For a given shaking level, any two slopes that have the same critical acceleration will yield the same Newmark displacement, regardless of how those slopes might differ in geometry or material properties. The critical-acceleration map portrays a measure of intrinsic slope properties independent of any ground-shaking scenario; thus, it is a map of seismic landslide susceptibility. We (Jibson et al., 1998) published such a map for the entire Oat Mountain 7 1/2′ quadrangle previously.

5.3. Estimating Newmark displacements

A rigorous Newmark analysis is conducted by double integrating the parts of a specific strong-motion record that exceed the critical acceleration. For a regional hazard analysis, conducting a rigorous Newmark analysis in each 10 m grid cell is both impractical and inappropriate. For each grid cell, a unique strong-motion record would have to be procured or artificially produced, and such a record would model only one of a broad range of possible ground-shaking levels.

To facilitate using Newmark's method in regional analysis, Jibson (1993) developed a sim-

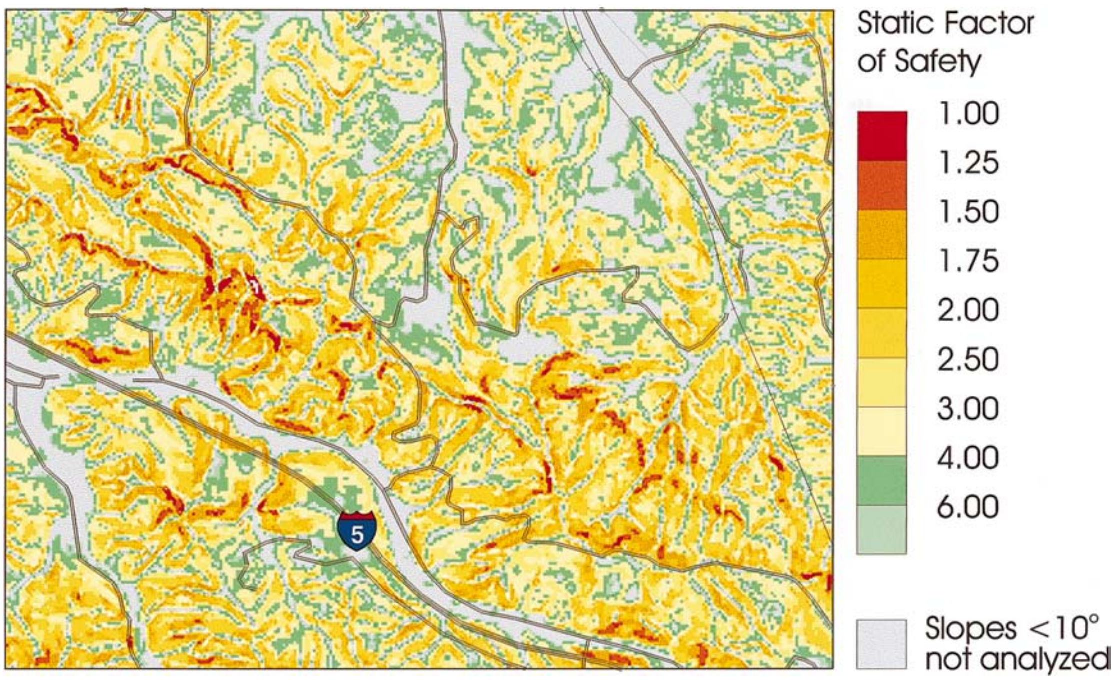

Fig. 9. Static factor-of-safety map of part of the Oat Mountain quadrangle (location shown in Fig. 3).

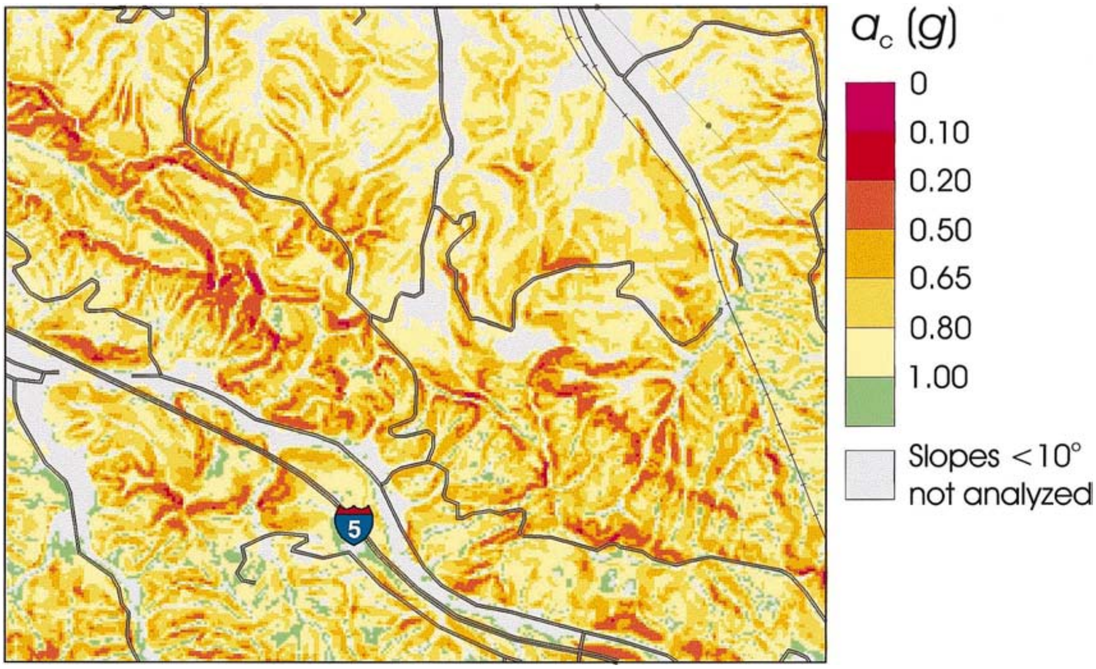

Fig. 10. Map showing susceptibility to seismically triggered landslides in part of the Oat Mountain quadrangle (location shown in Fig. 3). Susceptibility is portrayed in terms of critical acceleration (a_c).

plified Newmark method wherein an empirical regression equation is used to estimate Newmark displacement as a function of shaking intensity and critical acceleration. We slightly modified the functional form of that equation to make the critical-acceleration term logarithmic, and we used a much larger group of strong-motion records280 recording stations in 13 earthquakes (Table 2) to develop a new regression equation. (With this larger data set, a logarithmic critical-acceleration term yielded a much better fit than a linear term.) We analyzed both of the horizontal components of acceleration from 275 of the recordings and a single component from the remaining five, which yielded 555 single-component records. For each record, we determined the Arias (1970) intensity, a single numerical measure of the shaking intensity of the record calculated by integrating the squared acceleration values (Jibson, 1993). Then, for each strong-motion record, we conducted a rigorous Newmark analysis for several values of critical acceleration, ranging from 0.02 to 0.40*g*. The resulting Newmark displacements were then regressed on two predictor variables: critical acceleration and Arias intensity. The resulting regression equation is

$$\log D_n = 1.521 \log I_a - 1.993 \log a_c - 1.546, \qquad (3)$$

Table 2
Sources of strong-motion records used to model Newmark displacement

Earthquake	Magnitude	Recording stations	Components analyzed
Loma Prieta, 1989	7.1	29	57
Imperial Valley, 1979	6.5	22	44
Superstition Hills, 1987	6.5	12	24
Kern County, 1952	7.5	2	3
Daly City, 1957	5.3	1	2
Parkfield, 1966	6.1	3	6
San Fernando, 1971	6.6	2	3
Hilo, 1975	7.2	1	1
Santa Barbara, 1978	5.1	1	1
Tabas, Iran, 1978	7.4	1	2
Coyote Lake, 1979	5.8	11	22
Whittier Narrows, 1987	6.0	6	12
Northridge, 1994	6.7	189	378

where D_n is Newmark displacement in centimeters, I_a is the Arias intensity in meters per second, and a_c is the critical acceleration in *g*s. The regression equation is well constrained ($R^2 = 83\%$) with a very high level of statistical significance (>99%), and the model standard deviation is 0.375. Thus, Newmark displacement, an index of seismic slope performance, can be estimated as a function of critical acceleration (dynamic slope stability) and Arias intensity (ground-shaking intensity).

The distribution of landslides triggered by the Northridge earthquake was used to calibrate the modeling procedure; therefore, we produced a ground-shaking grid from the Northridge earthquake. For each of 189 strong-motion recordings of the mainshock, we plotted the average Arias intensity from the two horizontal components. We then used a simple kriging algorithm to interpolate values across a regularly spaced grid (Fig. 11).

Newmark displacements from the Northridge earthquake were estimated in each grid cell of the six quadrangles (Fig. 12) by using Eq. (3) to combine corresponding grid values of critical acceleration and Arias intensity. Predicted displacements range from 0 to 5256 cm.

5.4. *Estimating probability of failure*

Predicted Newmark displacements do not necessarily correspond directly to measurable slope movements in the field; rather, modeled displacements provide an index to correlate with field performance. For the Newmark method to be useful in a predictive sense, modeled displacements must be quantitatively correlated with field performance. In short, do larger predicted displacements relate to greater incidence of slope failure? Comparison of the predicted Newmark displacements (Fig. 12) with the actual inventory of landslides triggered by the Northridge earthquake (Fig. 13) allows us to answer this question.

The Newmark-displacement grid cells were grouped into bins, such that all cells having displacements between 0 and 1 cm were in the first bin; those having 1–2 cm of displacement were in the second bin, and so on. For displacements greater than about 10 cm, the number of cells in 1 cm bins became very small; therefore, broader ranges of displacement were grouped together to provide a statistically significant number of cells in each bin. For each bin, the proportion of the

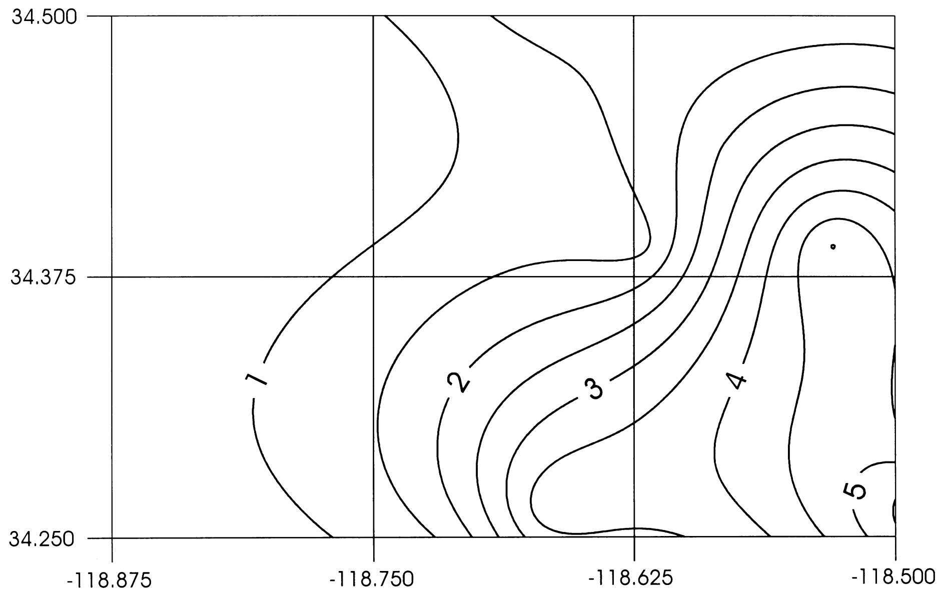

Fig. 11. Contours of Arias intensity (I_a) generated by the 1994 Northridge earthquake in the six quadrangles in the study area. Intensity values shown are in meters per second and are the averages of the two horizontal components.

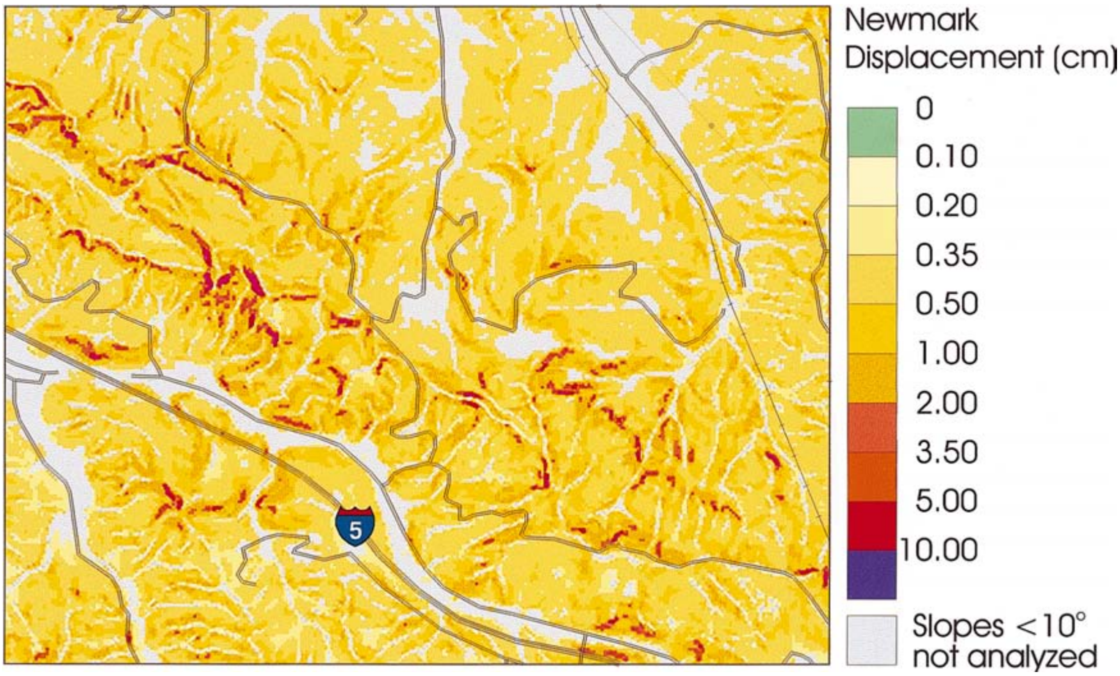

Fig. 12. Map showing predicted Newmark displacements in part of the Oat Mountain quadrangle (location shown in Fig. 3).

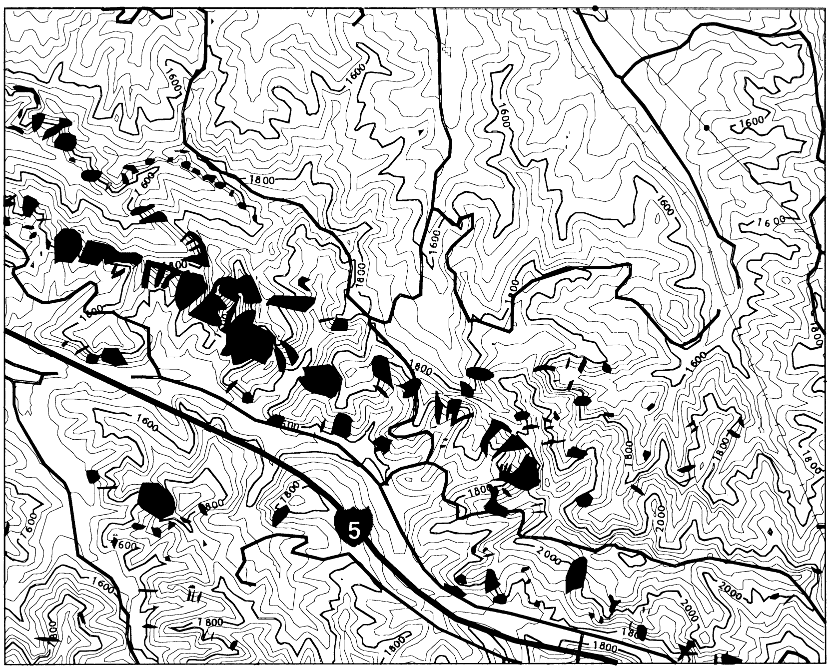

Fig. 13. Map showing landslides triggered by the 1994 Northridge earthquake (Harp and Jibson, 1995) in part of the Oat Mountain quadrangle (location shown in Fig. 3).

cells that were in landslide source areas was calculated. Landslide source areas were defined to include those grid cells having elevations above the median elevation for each landslide, so that the upper half of each landslide was considered a source area.

Fig. 14 shows, for each bin, the proportion of cells occupied by landslide source areas plotted as a function of Newmark displacement. The data clearly demonstrate the utility of Newmark's method to predict the spatial density of seismically triggered landslides: the proportion of landslide cells within each displacement bin increases almost monotonically with increasing Newmark displacement. The proportion of landslide cells increases rapidly in the first few centimeters (bins) of Newmark displacement and then levels off abruptly in the 10- to 15 cm range at a proportion of about 34%. This relation is critical in a predictive sense because the proportion of landslide cells in a given displacement bin is a direct estimate of the probability or percent chance that any cell in that displacement range will be occupied by a landslide source.

We chose to fit the data in Fig. 14 with a Weibull (1939) curve, which was initially developed to model the failure of rock samples (Jaeger and Cook, 1969). The functional form produces an S-shaped curve that is apparent in the data:

$$P(f) = m[1 - \exp(-aD_{\mathrm{n}}^{b})], \tag{4}$$

where $P(f)$ is the proportion of landslide cells, m is the maximum proportion of landslide cells indicated by the data, D_{n} is the Newmark displacement in centimeters, and a and b are the regression constants to be determined. The expression inside the brackets takes the form of the original Weibull equation, which yields values ranging from 0 to 1; the m outside the brackets simply scales this range to reflect the range represented by the data. The regression curve based on the Northridge data is

$$P(f) = 0.335[1 - \exp(-0.048D_{\mathrm{n}}^{1.565})]. \tag{5}$$

The curve fits the data extremely well ($R^2 = 97\%$), and prediction of the proportion of landslide cells [$P(f)$] can be used to directly estimate probability of slope failure as a function of Newmark displacement. This equation takes the same form as our previously published equation (Jibson et al., 1998) but has slightly different coefficients owing to the larger calibration data set used here. Once calibrated, the curve and corresponding equation can be used in any set of ground-shaking conditions to predict the probability of slope failure as a function of predicted Newmark displacement.

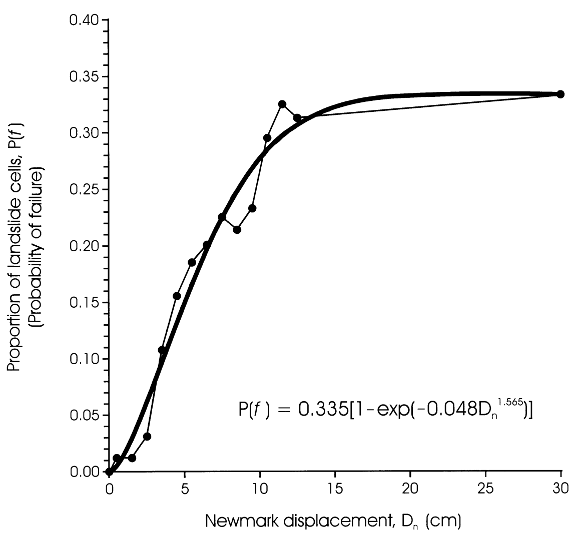

Fig. 14. Proportion of landslide cells as a function of Newmark displacement. Data are indicated by dots with a connecting line; the bold line is the best fit of the Weibull function shown in the figure [see Eqs. (4) and (5)].

5.5. Producing seismic landslide hazard maps

Fig. 14 and Eq. (5) provide the necessary linkage between the displacements estimated from the Newmark model and probabilities of landslide occurrence in the field. The curve thus forms the basis for producing seismic landslide hazard maps, which portray spatial variation in slope-failure probability in a specified set of ground-shaking conditions. Fig. 15 shows such a map for a part of the Oat Mountain quadrangle for the ground-shaking conditions experienced in the Northridge earthquake. Northridge-triggered landslides also are shown to demonstrate how well the mapping procedure captured what actually happened. The fit appears to be very good: most of the triggered landslides lie in the higher probability (warmer colored) areas, and most such areas contain land-

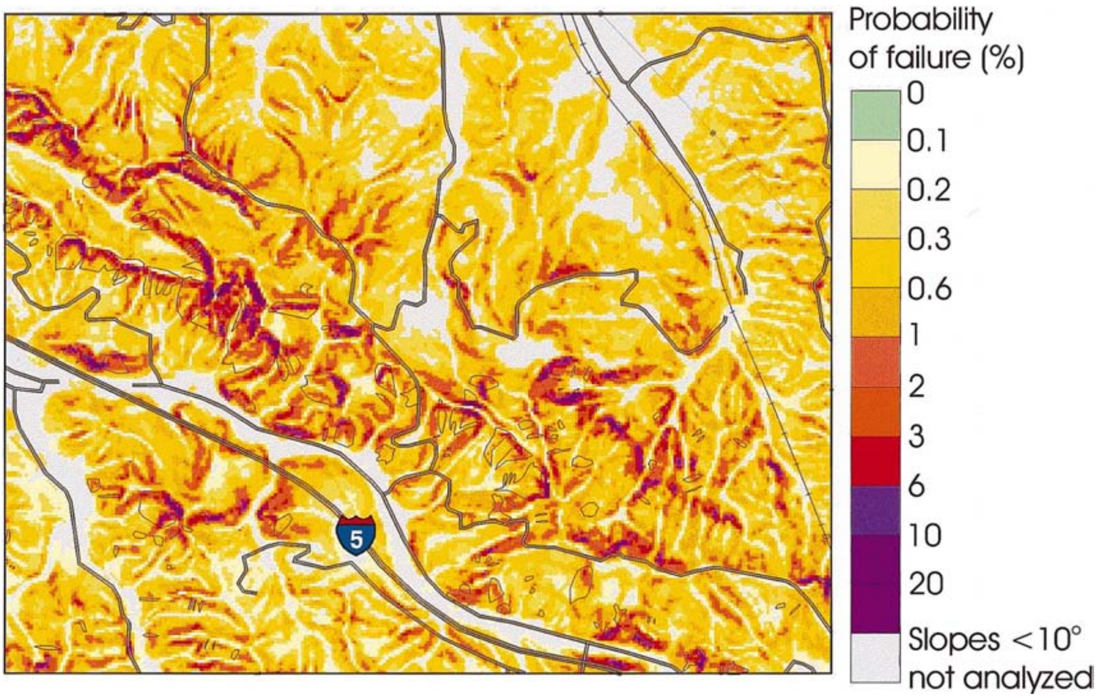

Fig. 15. Map showing probability of seismic triggering of landslides in Northridge-earthquake shaking conditions in part of the Oat Mountain quadrangle (location shown in Fig. 3).

slides. A hazard map of the entire Oat Mountain quadrangle (based on an earlier model calibration) has been published previously (Jibson et al., 1998)

Constructing a hazard (probability) map for other ground-shaking scenarios is equally straightforward, provided the ground-shaking can be reasonably modeled. Such a procedure would involve the following:

1. Specify the ground-shaking conditions in terms of Arias intensity. This could be a uniform level of shaking (for example, representing a 50 yr expected maximum shaking level) or shaking generated from a hypothetical earthquake of specified magnitude and location. Simple equations relating Arias intensity to other measures of ground-shaking (peak ground acceleration, magnitude and distance, etc.) have been published elsewhere (Wilson and Keefer, 1985; Jibson, 1993; Wilson, 1993).
2. Combine the shaking intensities with the critical-acceleration grid using Eq. (3) to estimate Newmark displacements.
3. Estimate failure probabilities from the Newmark displacements using Eq. (5).

6. Discussion

In our earlier paper (Jibson et al., 1998), we calibrated the probability model using data from the Oat Mountain 7 1/2′ quadrangle. The recalibration using six quadrangles in this paper stemmed primarily from our concern that data from a single quadrangle near the epicenter would not adequately account for attenuation of strong shaking at more distant locations. Interestingly, the calibration did not change greatly: the original functional form still fit the data well, and the coefficients did not change radically. The maximum proportion of cells failing increased from about 27% in the original calibration to 33.5% in the current calibration, which indicates increased predictive capability for the larger data set.

Nearly all of the variability in failure probability

(Fig. 14) occurs in the first few centimeters of displacement; for displacements greater than about 15 cm, no measurable increase in failure probability is predicted. This is perhaps attributable to the fact that the vast majority of landslides in the database were shallow, disrupted rock falls and rock slides in fairly brittle, weakly cemented sediments that fail at relatively small displacements. The shape of the curve strongly suggests brittle failure: most of what is going to fail does so within a narrow and relatively low range of displacements.

A maximum proportion of failed slopes of about 33% is reasonable in light of our experience in documenting triggered landslides in numerous world-wide earthquakes. Even on the most susceptible slopes in epicentral areas, we have rarely seen more than a quarter to a third of slope areas fail. In terms of slope area, a failure rate of 25–35% is catastrophic.

The overwhelming majority of landslides triggered by the Northridge earthquake were relatively shallow, disrupted slides and falls in rock and debris (Harp and Jibson, 1995, 1996). Therefore, any model calibrated from these data is useful primarily for predicting the spatial distribution of these types of landslides. The small number of deeper, more coherent slides triggered by the Northridge earthquake did not produce a statistically significant sample that could meaningfully contribute to the model. Thus, the distribution of deep, coherent landslides will probably be less accurately predicted using this calibration [Eq. (5)] than will the distribution of shallow, disrupted slides. Indeed, in most world-wide earthquakes, disrupted landslides are by far the predominant landslide type (Keefer, 1984), and so landslide distributions predicted using this method and calibration should relate well to typical distributions of triggered landslides.

As discussed previously, shear strengths used in the model reflect peak strengths in order to render the model statically stable. Relative strengths between units, however, are much more important than the absolute strength values, and relative strengths are reasonably well constrained. The calibration [Eq. (5)] is based on the strengths selected, and that calibration is only rigorously valid for models using the strengths in this paper. Using reduced strengths, either to represent residual-strength conditions or to simply take a more conservative approach, will not yield accurate results using Eq. (5). To appropriately use different strengths, the model would have to be recalibrated, which presumably would yield an equation similar to Eq. (5) but having different coefficients and exponents.

Shear strength typically has large spatial variability in nature even within geologic units, and assigning representative shear strengths to entire units is fraught with uncertainty. The modeling procedure, however, is heavily slope-driven. The effects of slope angle on the model output far outweigh the effects of modest differences in material strength; therefore, highly accurate characterizations of strength are not deemed essential. For example, the slight differences in strength between the different late Tertiary, weakly cemented units (Table 1) are virtually insignificant in terms of the model output. The much larger strength difference between these units and the well-cemented Chatsworth Formation, however, is very significant. Thus, assignment of strengths is primarily important in differentiating units having large strength differences.

The probability equation can be applied using any set of ground-shaking conditions of interest. The equation was calibrated using data from southern California, however, and applying it to regions that have greatly differing climates, rock types, vegetation, or topography increases the uncertainty of the results. Recalibration for use in different regions is desirable, but data sets for such calibration are generally lacking. Therefore, if this method is applied in other regions using Eq. (5), greater uncertainty in the output must be assumed. Values of a, b, and m [Eqs. (4) and (5)] could differ in other regions if the strengths of geologic materials, topography, vegetation, or soil moisture conditions were significantly different from those in southern California. In regions where the predominant failure type is different, the shape of the curve (Fig. 14) would probably be somewhat different as well. For example, if slumps and block slides in more compliant (less brittle) materials were predominant, the curve would likely be less steep and could flatten out at a larger maximum displacement value.

Maps produced using the method documented in this paper can be useful in emergency preparedness planning, lifeline siting and maintenance, critical-facility siting, long-term land-use planning, and a variety of other applications. Maps using this method, however, do not supersede published regulatory maps, such as the seismic hazard zonation maps issued by the California Division of Mines and Geology.

7. Summary and conclusion

Analysis of data from the Northridge earthquake allows quantitative physical modeling of conditions leading to coseismic slope failure. If data sets describing the topography, geology, shear strength, and seismic shaking of an area or region can be procured, the procedure described in this paper can be used to produce hazard maps showing the spatial distribution of slope-failure probability. Within the limitations discussed, such maps can find useful applications in regional seismic hazard and risk assessment.

Even considering all of the caveats and limitations discussed, this analytical mapping procedure provides a simple, systematic, physically based method to estimate seismic slope-failure probability. The linkage of Newmark displacement to a discrete failure probability is an enormously useful tool that will give Newmark's well-established method of analysis far more practical utility.

Acknowledgements

The Los Angeles County Department of Public Works and Leighton and Associates provided extensive data on material shear strengths. David Perkins and William Savage of the US Geological Survey provided helpful insights into the statistical modeling of the failure data. David Keefer, Ray Wilson, and Arthur Tarr of the US Geological Survey and an anonymous reviewer reviewed the manuscript. Graphic design and layout were prepared by Eleanor M. Omdahl and Pamela S. Detra.

References

Arias, A., 1970. A measure of earthquake intensity. In: Hansen, R.J. (Ed.), Seismic Design for Nuclear Power Plants. Massachusetts Institute of Technology Press, Cambridge, MA, pp. 438–483.

Harp, E.L., Jibson, R.W., 1995. Inventory of landslides triggered by the 1994 Northridge, California earthquake. In: US Geol. Surv. Open-File Rep. 95-213, 17 pp.

Harp, E.L., Jibson, R.W., 1996. Landslides triggered by the 1994 Northridge, California earthquake. Seismol. Soc. Am. Bull. 86, 1B, S319–S332.

Jaeger, J.C., Cook, N.G.W., 1969. Fundamentals of Rock Mechanics. Methuen and Company, London. 513 pp.

Jibson, R.W., 1993. Predicting earthquake-induced landslide displacements using Newmark's sliding block analysis. Transport. Res. Rec. 1411, 9–17.

Jibson, R.W., Harp, E.L., Michael, J.A., 1998. A method for producing digital probabilistic seismic landslide hazard maps: An example from the Los Angeles California area. US Geol. Surv. Open-File Rep. 98-113. 17 pp.

Keefer, D.K., 1984. Landslides caused by earthquakes. Geol. Soc. Am. Bull. 95, 406–421.

Morton, D.M., 1975. Seismically triggered landslides in the area above the San Fernando Valley. In: Oakeshott, G.B. (Ed.), San Fernando, California, Earthquake of 9 February 1971. California Division of Mines and Geology Bull. 196, 145–154.

Newmark, N.M., 1965. Effects of earthquakes on dams and embankments. Geotechnique 15, 139–160.

Parise, M., Jibson, R.W., 1997. Preliminary analysis of landslides triggered by the January 17 1994, Northridge earthquake in the Santa Susana quadrangle, California. US Geol. Surv. Open-File Rep. 97-719. 12 pp.

Weibull, W., 1939. In: Statistical Theory of the Strength of Materials. Ingenioersvetenskaps-akademien, Handlingar, Stockholm, p., 151.

Wieczorek, G.F., Wilson, R.C., Harp, E.L., 1985. Map showing slope stability during earthquakes in San Mateo County California. US Geol. Surv. Misc. Invest. Map I-1257-E, Scale 1:62,500.

Wilson, R.C., Keefer, D.K., 1983. Dynamic analysis of a slope failure from the 6 August 1979 Coyote Lake, California, earthquake. Seismol. Soc. Am. Bull. 73, 863–877.

Wilson, R.C., Keefer, D.K., 1985. Predicting areal limits of earthquake-induced landsliding. In: Ziony, J.I. (Ed.), Evaluating Earthquake Hazards in the Los Angeles Region — An Earth-science Perspective. US Geol. Surv. Prof. Paper 1360, 316–345.

Wilson, R.C., 1993. Relation of Arias intensity to magnitude and distance in California. US Geol. Surv. Open-File Rep. 93-556. 42 pp.

Yerkes, R.F., Campbell, R.H., 1993. Preliminary geologic map of the Oat Mountain 7.5′ quadrangle, southern California. US Geol. Surv. Open-File Rep. 93-525. 13 pp.

Yerkes, R.F., Campbell, R.H., 1995a. Preliminary geologic map of the Newhall 7.5′ quadrangle, southern California. US Geol. Surv. Open-File Rep. 95-503. 12 pp.

Yerkes, R.F., Campbell, R.H., 1995b. Preliminary geologic map of the Newhall 7.5′ quadrangle, southern California: a digital database. US Geol. Surv. Open-File Rep. 95-800.
Yerkes, R.F., Campbell, R.H., 1995c. Preliminary geologic map of the Oat Mountain 7.5′ quadrangle, southern California: a digital database. US Geol. Surv. Open-File Rep. 95-89.
Yerkes, R.F., Campbell, R.H., 1995d. Preliminary geologic map of the Piru 7.5′ quadrangle, southern California:. US Geol. Surv. Open-File Rep. 95-511. 6 pp.
Yerkes, R.F., Campbell, R.H., 1995e. Preliminary geologic map of the Piru 7.5′ quadrangle, southern California: a digital database. US Geol. Surv. Open-File Rep. 95-801.
Yerkes, R.F., Campbell, R.H., 1995f. Preliminary geologic map of the Simi 7.5′ quadrangle, southern California. US Geol. Surv. Open-File Rep. 95-828. 10 pp.
Yerkes, R.F., Campbell, R.H., 1995g. Preliminary geologic map of the Val Verde 7.5′ quadrangle, southern California. US Geol. Surv. Open-File Rep. 95-504. 9 pp.
Yerkes, R.F., Campbell, R.H., 1995h. Preliminary geologic map of the Val Verde 7.5′ quadrangle, southern California: a digital database. US Geol. Surv. Open-File Rep. 95-699.
Yerkes, R.F., Campbell, R.H., 1997a. Preliminary geologic map of the Santa Susana 7.5′ quadrangle, southern California. US Geol. Surv. Open-File Rep. 97-258. 11 pp.
Yerkes, R.F., Campbell, R.H., 1997b. Preliminary geologic map of the Santa Susana 7.5′ quadrangle, southern California: a digital database. US Geol. Surv. Open-File Rep. 97-258.
Yerkes, R.F., Campbell, R.H., 1997c. Preliminary geologic map of the Simi 7.5′ quadrangle, southern California: a digital database. US Geol. Surv. Open-File Rep. 97-259.